IEEE Access
Multidisciplinary ⋮ Rapid Review ⋮ Open Access Journal

Received January 24, 2022, accepted February 2, 2022, date of publication February 7, 2022, date of current version February 15, 2022.

Digital Object Identifier 10.1109/ACCESS.2022.3149527

Simultaneous Estimation of Unknown Road Roughness Input and Tire Normal Forces Based on a Long Short-Term Memory Model

SUNG JIN IM[1], JONG SEOK OH[2], AND GI-WOO KIM[1]
[1]Department of Mechanical Engineering, Inha University, Incheon 22212, South Korea
[2]Department of Future Automotive Engineering, Kongju National University, Cheonan 31080, South Korea

Corresponding authors: Jong Seok Oh (jongseok@kongju.ac.kr) and Gi-Woo Kim (gwkim@inha.ac.kr)

This work was supported by the Inha University Research Grant.

ABSTRACT This paper reports an initial study on the simultaneous estimation of unknown road roughness input and tire normal forces for automotive vehicles using a long short-term memory (LSTM) model. Active safety systems and the improvement of ride comfort using vehicle information have garnered increasing attention in the automotive industry. In particular, active safety systems rely significantly on road roughness data and the normal force of the tires. If these factors can be measured in real-time for a driving vehicle, the measured data can be used for automotive control systems for tasks, such as semi-active and active suspension control, rolling motion control, and torque vectoring. However, it is typically difficult to measure the road roughness and tire normal force directly in real-time by mounting physical sensors on the vehicle. In this study, we explore the simultaneous estimation of these factors using an LSTM model that requires only time-series data of the vehicle body. The LSTM model is implemented by using MATLAB/Simulink and includes data preprocessing, learning, and verification steps. To evaluate the estimation performance of the LSTM model, we compared it with a Kalman filter and used CarSim vehicle simulation software to simulate and interpret the dynamic behavior of vehicles.

INDEX TERMS Long short-term memory model, discrete Kalman filter-unknown input, 7-DOF full-car suspension model, tire normal forces, road roughness.

I. INTRODUCTION

Robust vehicle control is necessary to improve vehicle safety and performance and has drawn considerable research interest in recent years. In particular, active safety systems have been recently developed using chassis information from vehicles to improve driver's comfort and safety [1]. For example, the active body control (ABC) system, including the active roll stabilizer (ARS) system and active damper system, can be governed by the characteristics of vehicle vertical dynamics. These control systems are designed to enhance the turning stability of the vehicle and reduce vibrations in the vehicle body due to the irregularity of road inputs; therefore, the road roughness (frequently referred to as road profile) and tire normal force plays a key role in designing these controllers because they act as unknown disturbance inputs to the control system [2], [3]. However, many previous studies for active body control system has considered only the vertical motion of sprung mass such as vertical speed or acceleration due to the difficulty in real-time estimation of road roughness and tire normal force [4]. The real-time information on road roughness can significantly improve the comfort and safety of autonomous vehicles because road roughness also can serve as a reference index for autonomous path planning [5].

Road roughness can be measured directly using a laser sensor or an optical device, such as a camera or a light detection and ranging (LIDAR) system [6], [7]. However, in the case of direct measurement methods, it is inconvenient to install expensive sensors. Furthermore, the algorithm of the 3D imaging method is generally complicated, resulting in a high computational burden. Thus, some researchers proposed an alternative method of road roughness estimation using a Kalman filter based on the measured system response due to the disturbance applied to the vehicle system. Several

The associate editor coordinating the review of this manuscript and approving it for publication was Wentao Fan.

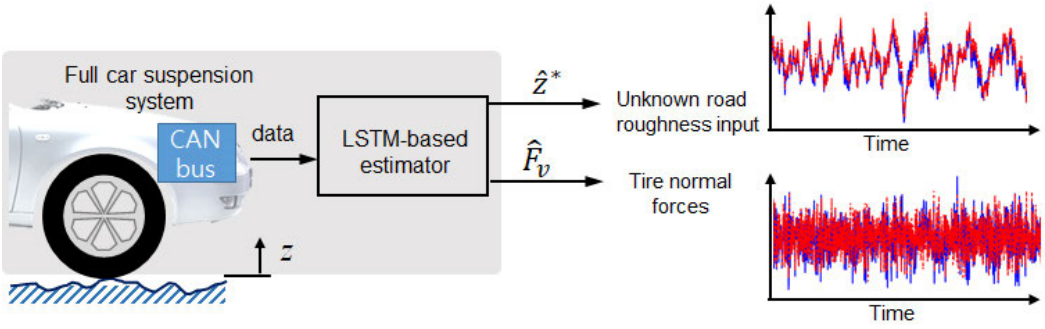

FIGURE 1. Overall schematic of the simultaneous estimation of unknown road input and tire normal force using LSTM-based estimator (model).

researchers have studied Kalman filters to estimate road roughness. For example, Kang *et al.* applied this algorithm for estimating road roughness [8]. Kim *et al.* estimated the state information of the suspension control system and validated its performance [9]. From these studies, the DKF–UI algorithm has been known as an effective algorithm to address the estimation problem with unknown input and state information, as it does not require any prior information.

Recently, data-driven engineering approaches have been introduced as an alternative approach for estimating unknown inputs and state information. In the data-driven approach, a highly nonlinear mapping from the input to the output data is learned during an offline training process. There are several inherent advantages of adopting a data-driven approach. First, the model learns the dynamics of the system directly from the data; thus, the need for explicit physical modeling is not necessary. Second, the forward-path for evaluating a pre-trained deep neural network consists solely of basic operations and nonlinear activation functions. Hence, it is computationally efficient compared with a model-based Kalman filter algorithm. Previous data-driven approaches have focused solely on estimating road roughness. Some studies have attempted to classify road roughness using machine-learning algorithms [10], [11]. A previous study used a fuzzy model along with a static nonlinear autoregressive exogenous (NARX) model to successfully estimate the road roughness using simulated data [12], while a further study validated the performance of the NARX model with field-test results [13]. To estimate the unknown road roughness and four system states, Kim *et al.* proposed a new encoder-decoder structured recurrent neural network (RNN) model with a two-phase attention mechanism to better characterize the dynamic behavior of suspension systems [14].

Although the vehicle normal force of a road on a tire at the contact patch can be used in many vehicular control applications (e.g., active roll control to prevent the rollover), there were few types of research because the measurements of tire normal force are challenging. Because the use of physical sensors to directly measure the normal force of an automotive tire is expensive and impractical [15], many analytical and experimental studies have investigated the use of virtual sensors (i.e., sensor data fusion) for the indirect measurement of tire force. For example, the longitudinal and lateral tire force history and vehicle conditions were estimated using an EKF-based 9-DOF vehicle model [16]. However, the estimator did not determine the normal force of each tire because it used a half-car model. Samadi *et al.* estimated the longitudinal tire forces per wheel and lateral tire forces per axle using a square root EKF-based four-wheel vehicle model with a Gauss–Markov model for friction [17]. Doumiati *et al.* used EKF to estimate the normal forces of each tire, regardless of the tire model [18]. However, it was assumed that the vehicle was traveling on a flat road with no irregularities on the road surface.

Based on the individual studies on the estimation of road roughness and vehicle's several state variables, the simultaneous estimation of road roughness and state variables has been recently attempted to alleviate the computational complexity. The simultaneous estimation of tire normal forces and road roughness enables dynamic interpretation of the vehicle system considering road roughness and improves the driving force distribution and control performance of the brake system [19], [20]. Tsunashima *et al.* designed an estimator using multiple interacting models considering the vehicle's internal state and road state simultaneously from the measurement of the lateral acceleration and yaw rate [21]. Rath *et al.* simultaneously estimated the road roughness and tire road friction of the quarter car system using higher-order sliding mode and nonlinear Lipshitz observer [22]. Wang *et al.* used the adaptive unscented Kalman filter to classify various road conditions while estimating the vehicle state [23]. Because previous studies [19]–[23] are associated with physical model-based simultaneous estimation, physical model inaccuracy leads to low estimation performance. Recently, Kim *et al.* estimated the road roughness and vehicle state based on model-free prediction such as a deep-learning-based observer system [14]. The sequence data calculation input to the offline pre-trained deep-learning model consists of only the calculated nonlinear activation function, resulting in a small computational burden compared with the Kalman filter. Although previous studies have shown promising results in estimating road roughness and state variables, the following issues should be further considered.

- The simultaneous estimation of the road roughness and tire normal force is required for full-car control-system applications because it plays a key role in designing these controllers such as ABC and ARS.
- The number of sensors should be minimized from the viewpoint of cost-effectiveness and simplicity because the use of multiple sensors results in complex and expensive chassis-control systems.

Therefore, the objective of this study is to explore a new method for estimating the tire normal force and unknown road input simultaneously based on a deep-learning estimation system called the long short-term memory (LSTM) model, as described schematically in Figure 1. To evaluate the performance of the proposed method, we designed a DKF–UI model based on [8] and compared it with the LSTM model. CarSim®(V 9.0) vehicle simulation software was used as a full-vehicle dynamics simulator to generate vehicle sensor data used as the learning and test data. It was also used for the validation of the LSTM model because it has been widely used as an accurate alternative platform to real-world in-vehicle tests [24]. To validate the LSTM model, we additionally performed physical-model-based simulations considering the vertical and longitudinal dynamics of the seven degree-of-freedom (DOF) vehicle model.

II. DATA-DRIVEN ENGINEERING APPROACH

A. OVERVIEW OF LSTM MODEL

The LSTM model was initially proposed for the deep learning application with time-series data such as speech, sentences, and video [25]. LSTM can maintain both long-term and short-term memory and is a type of recurrent neural network (RNN). It introduces a structure called a gate and memory cell. This structure allows the model to inherit only the information needed at the next point in time while determining the amount of historical information that needs to be remembered. Figure 2 shows a schematic of the proposed data-driven engineering approach for simultaneously estimating the unknown road input and tire normal force using the LSTM model. The unknown road roughness acts as an input to the CarSim model. Five sensor data points were acquired from the CarSim model and used as measured values for input into a pre-trained LSTM model. The LSTM has a circular structure similar to an RNN and has a complex internal structure. The LSTM cell has three gates and one memory cell, where x_t is the input, h_t is the output at time t, and h_{t-1} is the output immediately before t and l denote the order of the LSTM cells. In Figure 2, arrows indicate the flow of data, and circles indicate operations between matrix elements. The number of cells represented by n is given by the total data divided by the window size. The forward-propagation process can be expressed as follows:

- Forget gate

$$f_t^{(l)} = \sigma(W_{xf}^{(l)} x_t + W_{hf}^{(l)} h_{t-1} + b_f^{(l)}) \tag{1}$$

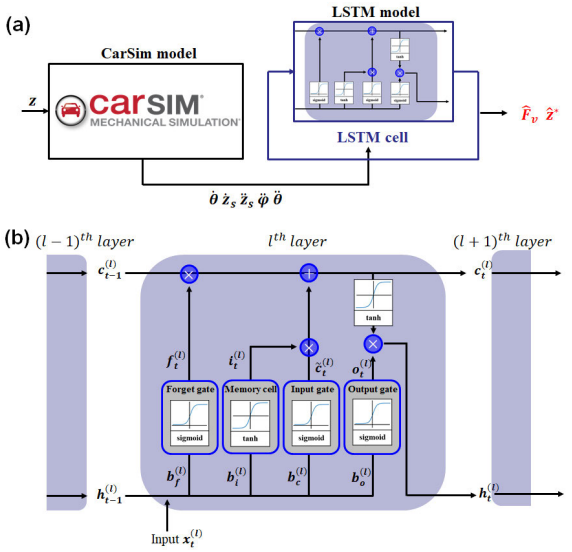

FIGURE 2. The proposed method for simultaneously estimating the road input and tire normal force using LSTM (a) overall schematic, (b) detail Internal structure of the LSTM model.

- Input gate and new memory

$$\begin{aligned} i_t^{(l)} &= \sigma(W_{xi}^{(l)} x_t + W_{hi}^{(l)} h_{t-1} + b_i^{(l)}) \\ \tilde{c}_t^{(l)} &= \tanh(W_{xc}^{(l)} x_t + W_{hc}^{(l)} h_{t-1} + b_c^{(l)}) \end{aligned} \tag{2}$$

- Output gate

$$o_t^{(l)} = \sigma(W_{xo}^{(l)} x_t + W_{ho}^{(l)} h_{t-1} + b_0^{(l)}) \tag{3}$$

- Cell state c_t and hidden state h_t

$$\begin{aligned} c_t^{(l)} &= f_t^{(l)} \circ c_{t-1}^{(l)} + i_t^{(l)} \circ \tilde{c}_t^{(l)} \\ h_t^{(l)} &= o_t^{(l)} \circ \tanh(c_t^{(l)}) \end{aligned} \tag{4}$$

The forget gate adjusts how much of the memory cell's contents are left behind. A sigmoid function is used for the forget gate. The output value h_{t-1} at the previous time and x_t entering the LSTM cell at the current time is multiplied by the weight and added to the bias b_f. This output value is used as the input for the sigmoid function. Here, f_t passing through the sigmoid activation function is multiplied by c_{t-1}, and the data then flows to the next step. The input gate adjusts how much of the output is reflected in the memory cell at time $t-1$. Then, i_t that passes the activation function *tanh* becomes a new memory that is added to the memory cell. A c_t is created by multiplying the new memory i_t by the $\tilde{c}_t$ passed input gate. The created c_t stores only the necessary information and is passed to the next LSTM cell. Finally, it remains to decide what to export as an output. This output is a filtered value based on the cell state. First, it decides which part of c_t to output as the input data to the sigmoid layer. Then, c_t is passed through the *tanh* layer and multiplied by the output of the sigmoid gate calculated earlier. Thus, the exported data contains only the desired portion as output h_t.

Figure 3 shows the expansion structure of the LSTM model and time series data learning process, where n is the number

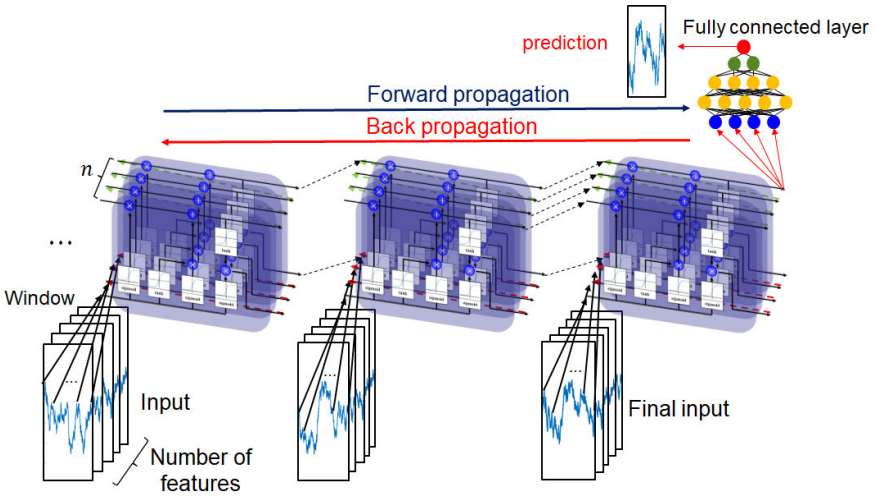

FIGURE 3. Extended structure of LSTM model showing the learning process of time series data.

of cells in the LSTM model, which is equal to the window size. The window has a fixed size in units for training the LSTM model. If there are 10 window data points, 10 previous data points are used to predict the value of the next time unit. For forward propagation, the output data is calculated through the fully connected layer. Training is then performed to determine all optimal weight values through the backpropagation.

B. TRAINING DATA ACQUISITION

All input data used for training were generated for a D-class sedan vehicle model with a driving speed of 60 km/h using CarSim. In this study, the tire model of Pacejka 5.2 is used with standardized magic formula model coefficients to represent visco-elastic properties of tires [26], [27]. A parallel-track road model was used, and the road elevation (i.e., road roughness, profile) on the left and right tracks were synthesized. Then, continuous data of the vehicle's response to this synthesized road input were obtained. Standard ISO 8608 specifies the road classification of longitudinal random road roughness based on the power spectral density (PSD) of vertical elevation [9]. In this study, the road roughness was synthesized for C-class roads (stationary roads). The slopes of the PSD graphs of the test roads were -1.94 and -1.86 respectively. These values are close to the value (-2) of the level road roughness classified as an international roughness index, as shown in Figure 4 [28].

In this study, only the input data of the sprung mass in CarSim were required for the use of deep learning. Thus, 6-D inertial measurement unit (IMU) sensors and accelerometers were used to measure the motion of the sprung mass. The 6-D IMU provides information on the vehicle's longitudinal acceleration (a_x), lateral acceleration (a_y), and yaw rate (ψ). Acceleration sensors are used to detect the vertical movement of a vehicle. We generated input data using sensors, and the output data were the four normal forces and the unknown road input of each tire from the learned model, as shown in Table 1. The input data for the LSTM model are the pitch

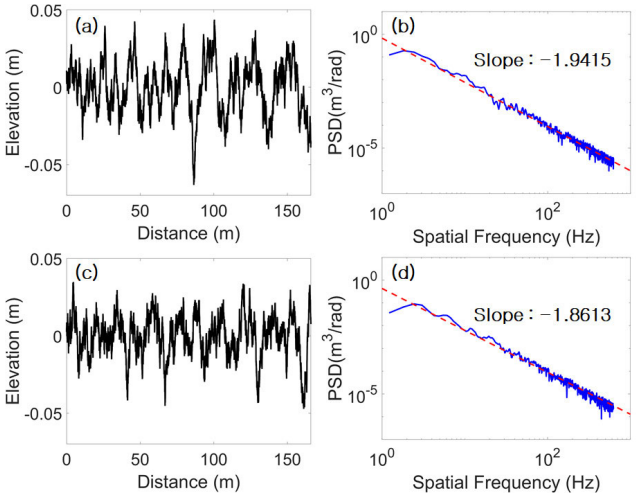

FIGURE 4. Synthesized road roughness profiles used as the unknown road input. (a), (c) road roughness of parallel tracks, and (b), (d) their corresponding PSD.

rate ($\dot{\theta}$), sprung mass vertical speed ($\dot{z}_s$), acceleration ($\ddot{z}_s$), roll acceleration ($\ddot{\varphi}$), pitch acceleration ($\ddot{\theta}$). To reduce the number of sensors, the proposed LSTM model only use an inertial measurement unit (IMU) and accelerometer, which have been successfully applied to the automotive industry because they are cost-effective and highly reliable. From the IMU such as gyro sensor and accelerometer, sprung mass acceleration along z-axis and roll and pitch rate were directly measured. Then, the integral with high-pass filtering for reducing the drift error and differential operations with low-pass filtering for removing electrical noises are implemented to acquire the sprung mass velocity and roll/pitch accelerations. The deep learning-based estimation method has the advantage that only the measured sensor data of the sprung mass are required.

The tire normal force and road roughness in the LSTM model was also estimated through training, verification, and testing processes. In this study, shuffle division

TABLE 1. Input and output data for LSTM model.

Model	Input data	Output data
LSTM	$\dot{\theta}[\deg/s]$ $\dot{z}_s[m/s]$ $\ddot{z}_s[m/s^2]$ $\ddot{\varphi}[\deg/s^2]$ $\ddot{\theta}[\deg/s^2]$	$F_{v1}[N]\, z_1[m]$ $F_{v2}[N]\, z_2[m]$ $F_{v3}[N]\, z_3[m]$ $F_{v4}[N]\, z_4[m]$

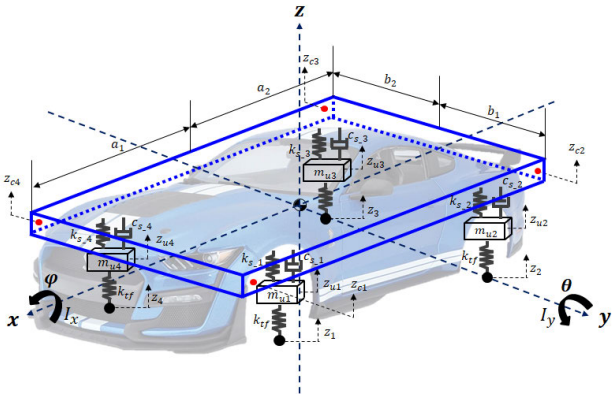

FIGURE 5. Schematic of full car suspension model (7-DOF).

cross-validation was used because it allows the alleviation of overfitting concerns and rapid operations for large data sets [29]. The hyper-parameters used for training were maximum epochs, initial learning rate, learning rate drop period, learning rate drop factor, and mini-batch size. An optimization algorithm called adaptive moment estimation (ADAM) is used to efficiently learn [30]. The hyper-parameters are discussed in detail in Section III-B.

III. PERFORMANCE VALIDATION

A. DKF-UI WITH TIRE NORMAL FORCE ESTIMATOR

In this study, the discrete Kalman filter–unknown input (DKF–UI) with tire normal force estimator is developed to validate the performance of LSTM. A 7-DOF full-car suspension model is used for the DKF-UI model, as shown in Figure 5 [31], [32]. This full-car model assumes that each wheel affects the springs and dampers of the other wheels. The wheel model consists of only weight and tire stiffness. Because the actual vehicle tire damping is very small compared to the tire stiffness, it is generally neglected.

The 7-DOF suspension model consists of four wheels moving vertically in the z-direction, a rotational moving body of the vehicle about the x-direction (roll motion), a rotational body of the vehicle about the y-direction (pitch motion), and a rotational body of the vehicle about the z-direction (yaw motion). The response of the vehicle system is caused by vertical excitation owing to the road disturbance applied to the four wheels. The road roughness input for the DKF-UI model is shown in Figure 4. The governing equation of the full-car suspension model is derived from Equations (5)∼(11)

$$\begin{aligned} m_s\ddot{z}_s = &-F_{c1} - F_{c2} - F_{c3} - F_{c4} - F_{ks1} \\ &-F_{ks2} - F_{ks3} - F_{ks4} - m_s g \end{aligned} \tag{5}$$

TABLE 2. Parameters for the full-car suspension model.

Symbol	Parameter	Value	Unit
m_s	Sprung mass	1370	kg
$m_{ui}(i=1,2,3,4)$	Unsprung mass	40	kg
I_x	Moment of inertia (rolling)	671.3	$kg{\cdot}m^2$
I_y	Moment of inertia (pitching)	1972.8	$kg{\cdot}m^2$
k_{tf}	Tire stiffness	240000	N/m
$k_{si}(i=1,2,3,4)$	Spring stiffness	30000	N/m
g	Gravitational acceleration	9.81	m/s^2
$c_{si}(i=1,2,3,4)$	Damping coefficient	3000	Ns/m
a_1	Vehicle length (forward)	1.11	m
a_2	Vehicle length (backward)	1.67	m
b_l	Vehicle width (left)	0.775	m
b_2	Vehicle width (right)	0.775	m

$$\begin{aligned} I_y\ddot{\theta} = &-a_1(-F_{c1} - F_{ks1}) - a_1(-F_{c4} - F_{ks4}) \\ &+a_2(-F_{c2} - F_{ks2}) + a_2(-F_{c3} - F_{ks3}) \end{aligned} \tag{6}$$

$$\begin{aligned} I_x\ddot{\varphi} = &\, b_1(-F_{c1} - F_{ks1}) + b_1(-F_{c2} - F_{ks2}) \\ &-b_2(-F_{c3} - F_{ks3}) - b_2(-F_{c4} - F_{ks4}) \end{aligned} \tag{7}$$

$$m_{u1}\ddot{z}_{u1} = F_{c1} + F_{ks1} - k_{tf}(z_{u1} - z_1) - m_{u1}g \tag{8}$$

$$m_{u2}\ddot{z}_{u2} = F_{c2} + F_{ks2} - k_{tf}(z_{u2} - z_2) - m_{u2}g \tag{9}$$

$$m_{u3}\ddot{z}_{u3} = F_{c3} + F_{ks3} - k_{tf}(z_{u3} - z_3) - m_{u3}g \tag{10}$$

$$m_{u4}\ddot{z}_{u4} = F_{c4} + F_{ks4} - k_{tf}(z_{u4} - z_4) - m_{u4}g \tag{11}$$

where m_s is the mass of the vehicle body, $m_{ui}(i = 1, 2, 3, 4)$ is the mass of each wheel, and I_x and I_y are the roll and pitch mass moments of inertia, respectively. In addition, k_{tf} is the tire stiffness, assuming that all four wheels have the same stiffness; z_s is the vertical displacement of the vehicle body mass; $z_{ui}(i = 1, 2, 3, 4)$ are the vertical displacements of each wheel; z_i $(i = 1, 2, 3, 4)$ are the unknown road inputs applied to each wheel; φ and θ are the roll and pitch angular displacements, respectively; and F_{ci} and $F_{ksi}(i = 1, 2, 3, 4)$ are the damping force and restoring force of each wheel, respectively. The state vectors and unknown input z^* are defined in Equations (12) and (13), respectively. The physical parameters for the full-car suspension model are listed in Table 2.

$$\begin{aligned} x &= \left[z_{u1}\ \dot{z}_{u1}\ z_{u2}\ \dot{z}_{u2}\ z_{u3}\ \dot{z}_{u3}\ z_{u4}\ \dot{z}_{u4}\ \varphi\ \dot{\varphi}\ \theta\ \dot{\theta}\ z_s\ \dot{z}_s \right]^T \\ &= \left[x_1\ x_2\ x_3\ x_4\ x_5\ x_6\ x_7\ x_8\ x_9\ x_{10}\ x_{11}\ x_{12}\ x_{13}\ x_{14} \right]^T \end{aligned} \tag{12}$$

$$z^* = \left[z_1\ z_2\ z_3\ z_4 \right]^T \tag{13}$$

Although a DKF–UI applied system should be a linear system and the input applied to the system is a known value, the DKF–UI model can be applied to estimate unknown road inputs using a random walk model. Kang estimated the unknown road input by applying the DKF–UI model to a quarter-car model [8]. In this study, four unknown road roughness values applied to each wheel of a full-car model were estimated using the DKF–UI model, and the normal force was indirectly estimated based on the estimated unknown road input. The following equations represent the main estimation process of the DKF-UI algorithm and the detail process is described in [8] and [9].

TABLE 3. Input and output data for DKF-UI model.

Model	Input data	Output data
DKF-UI	$z_s[m]$ $\ddot{z}_s[m/s^2]$ $\ddot{\varphi}[\deg/s^2]$ $\ddot{\theta}[\deg/s^2]$ $\ddot{z}_{u1}[m/s^2]$ $\ddot{z}_{u2}[m/s^2]$ $\ddot{z}_{u3}[m/s^2]$ $\ddot{z}_{u4}[m/s^2]$	$F_{v1}[N]\, z_1[m]$ $F_{v2}[N]\, z_2[m]$ $F_{v3}[N]\, z_3[m]$ $F_{v4}[N]\, z_4[m]$

- Initialization of parameter at $k = 0$

$$\begin{aligned} \hat{x}_0 &= E[x_0] \\ \hat{z}_0 &= E[z_0^*] \\ P_0 &= E\left[(x_0 - \hat{x}_0)(x_0 - \hat{x}_0)^T\right] \end{aligned} \tag{14}$$

$$S_0 = E\left[(z_0^* - \hat{z}_0^*)(z_0^* - \hat{z}_0^*)^T\right] \tag{15}$$

- Prediction step

$$\begin{aligned} \hat{x}(k|k-1) &= A_d\hat{x}(k-1) + B_d z(k-1) \\ P(k|k-1) &= A_d P(k-1)A_d^T + Q \end{aligned} \tag{16}$$

- Kalman gain calculation

$$K(k) = P(k|k-1)C^T(CP(k|k-1)C^T + R)^{-1} \tag{17}$$

- Unknown input estimation step

$$\begin{aligned} S(k) &= \left[D^T R^{-1}(I - CK(k))D\right]^{-1} \\ \hat{z}^*(k) &= S(k)D^T R^{-1}[I - (CK(k))][q(k) - C\hat{x}(k)] \end{aligned} \tag{18}$$

- Correction step

$$\begin{aligned} \hat{x}(k|k) &= \hat{x}(k|k-1) + K(k) \\ &\quad \times \left[q(k) - C\hat{x}(k|k-1) - D\hat{z}^*(k)\right] \\ P(k|k) &= \left[I + K(k)DS(k)D^T R^{-1}C\right] \\ &\quad \times [I - K(k)C]\,P(k|k-1) \end{aligned} \tag{19}$$

The input data for the DKF-UI model are the sprung mass vertical displacement z_s, $\ddot{z}_s$, $\ddot{\varphi}$, $\ddot{\theta}$, and unsprung mass acceleration of each tire $\ddot{z}_{ui}(i = 1, 2, 3, 4)$, as shown in Table 3. Several acceleration sensors, displacement sensors, and laser sensors are required to measure the unsprung mass data for DKF–UI model [8]. This is a disadvantage because several expensive sensors are required, which are inconvenient for installation inside vehicles. Figure 6 presents an overall flow diagram of the unknown road input estimation process. The notation $''$ represents the estimated value.

After estimating the unknown road roughness, the tire normal forces were estimated. The unknown road roughness acts as an input to the 7-DOF suspension system. The DKF–UI model estimates the input of 14 vehicle states and 4 unknown road inputs. The estimated data can be used to obtain the tire static normal force using a longitudinal vehicle model [33]. The dynamic tire normal force of the vehicle considering the longitudinal load transfer can be calculated using the tire normal force calculator. All parameters of the longitudinal

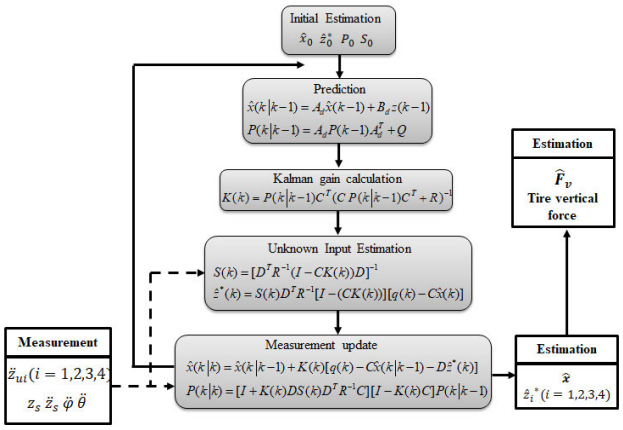

FIGURE 6. Overall flow chart for the DKF-UI model.

vehicle model are defined in Figure 7. The corresponding moment equilibrium equation is as follows.

$$\begin{aligned} \sum M_A &= N_r l - l_f mg + hma_x = 0 \\ \sum M_B &= -N_f l + l_r mg - hma_x = 0 \end{aligned} \tag{20}$$

where $\sum M_A$ and $\sum M_B$ denote the summations of the moments at points A and B, respectively; N_1 is the left front tire normal force; N_2 is the left rear tire normal force; N_3 is the right front tire normal force, and N_4 is the right rear tire normal force. Further, N_f is the sum of N_1 and N_3, and N_r is the sum of N_2 and N_4. In this study, it is assumed that the vehicle is traveling at a constant speed, and the acceleration a_x of the vehicle in the longitudinal direction is assumed to be zero. Therefore, the static tire normal force for each tire is determined as follows.

$$\begin{aligned} N_f &= \frac{l_r}{l}mg, \quad N_1 = N_3 = \frac{N_f}{2} \\ N_r &= \frac{l_f}{l}mg, \quad N_2 = N_4 = \frac{N_r}{2} \end{aligned} \tag{21}$$

The calculation of the dynamic tire normal force of the vehicle considering the load transfer is expressed as follows.

$$F_v = F_g + F_d + F_s + F_{ts} + F_{sv} \tag{22}$$

where F_g is the force considering the wheel load, F_d is the damping force, F_s is the restoring force, F_{ts} is the force due to tire stiffness, and F_{sv} is the static tire normal force. The dynamic normal forces of each tire are as follows.

$$F_v = \begin{bmatrix} F_{v1} & F_{v2} & F_{v3} & F_{v4} \end{bmatrix}^T \tag{23}$$

$$\begin{aligned} F_{v1} &= m_{u1}g + c_{s1}(\dot{z}_{c1} - \dot{z}_{u1}) \\ &\quad + k_{s1}(z_{c1} - z_{u1}) - k_{tf}(z_{u1} - z_1) + N_1 \end{aligned} \tag{24}$$

$$\begin{aligned} F_{v2} &= m_{u2}g + c_{s2}(\dot{z}_{c2} - \dot{z}_{u2}) \\ &\quad + k_{s2}(z_{c2} - z_{u2}) - k_{tf}(z_{u2} - z_2) + N_2 \end{aligned} \tag{25}$$

$$\begin{aligned} F_{v3} &= m_{u3}g + c_{s3}(\dot{z}_{c3} - \dot{z}_{u3}) \\ &\quad + k_{s3}(z_{c3} - z_{u3}) - k_{tf}(z_{u3} - z_3) + N_3 \end{aligned} \tag{26}$$

$$\begin{aligned} F_{v4} &= m_{u4}g + c_{s4}(\dot{z}_{c4} - \dot{z}_{u4}) \\ &\quad + k_{s4}(z_{c4} - z_{u4}) - k_{tf}(z_{u4} - z_4) + N_4 \end{aligned} \tag{27}$$

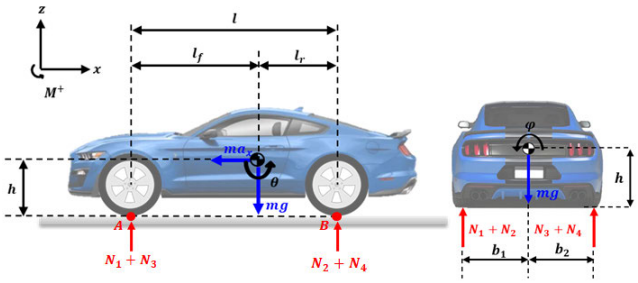

FIGURE 7. Longitudinal vehicle dynamics model.

TABLE 4. Tuning parameters for the DKF–UI model.

Item	Values
x_0	$[0\ 0\ 0\ 0\ 0\ 0\ 0\ 0\ 0\ 0\ 0\ 0\ 0\ 0]^T$
P_0,	$diag[1\ 1\ 1\ 1\ 1\ 1\ 1\ 1\ 1\ 1\ 1\ 1\ 1\ 1]$
Q	$diag[1\ 1\ 1\ 1\ 1\ 1\ 1\ 1\ 1\ 1\ 1\ 1\ 1\ 1]\times 10^{-14}$
R	$diag[1\ 1\ 1\ 1\ 1\ 1\ 1\ 1]\times 10^{28}$

$$z_c = \begin{bmatrix} z_{c1} & z_{c2} & z_{c3} & z_{c4} \end{bmatrix}^T = \begin{bmatrix} z_s + b_1\varphi - a_1\theta \\ z_s + b_1\varphi + a_2\theta \\ z_s - b_2\varphi + a_2\theta \\ z_s - b_2\varphi - a_1\theta \end{bmatrix} \quad (28)$$

where z_c is a vector represented by an element with a vertical displacement on each of the four sides of the suspension [38]. Finally, the dynamic tire normal force of each tire was estimated using the state and unknown road inputs estimated by the DKF–UI model.

$$\hat{F}_v = \begin{bmatrix} \hat{F}_{v1} & \hat{F}_{v2} & \hat{F}_{v3} & \hat{F}_{v4} \end{bmatrix}^T \quad (29)$$

$$\hat{F}_{v1} = m_{u1}g + c_{s1}(\dot{\hat{z}}_{c1} - \dot{\hat{z}}_{u1}) + k_{s1}(\hat{z}_{c1} - \hat{z}_{u1}) - k_{tf}(\hat{z}_{u1} - \hat{z}_1) + N_1 \quad (30)$$

$$\hat{F}_{v2} = m_{u2}g + c_{s2}(\dot{\hat{z}}_{c2} - \dot{\hat{z}}_{u2}) + k_{s2}(\hat{z}_{c2} - \hat{z}_{u2}) - k_{tf}(\hat{z}_{u2} - \hat{z}_2) + N_2 \quad (31)$$

$$\hat{F}_{v3} = m_{u3}g + c_{s3}(\dot{\hat{z}}_{c3} - \dot{\hat{z}}_{u3}) + k_{s3}(\hat{z}_{c3} - \hat{z}_{u3}) - k_{tf}(\hat{z}_{u3} - \hat{z}_3) + N_3 \quad (32)$$

$$\hat{F}_{v4} = m_{u4}g + c_{s4}(\dot{\hat{z}}_{c4} - \dot{\hat{z}}_{u4}) + k_{s4}(\hat{z}_{c4} - \hat{z}_{u4}) - k_{tf}(\hat{z}_{u4} - \hat{z}_4) + N_4 \quad (33)$$

B. SIMULATION SCHEME

The simulation of the entire vehicle model was performed assuming a vehicle traveling on a road at a certain velocity, where both the DKF–UI and LSTM model were implemented in MATLAB/Simulink® (solver of ode4 Runge-Kutta, step size of 0.001). For the DKF-UI model, the initial values of x_0 and P_0 are set before the algorithm is executed. Because it is difficult to set the initial values of the state vector and covariance matrix to realistic values, they are initially set to arbitrary values. The initial Q and R were updated using a trial-and-error process. The initial values of x_0, P_0, Q, and R are listed in Table 4.

For the LSTM model, many hyper-parameters need to be adjusted by the user. Six hyper-parameters were used in this study, as listed in Table 5. The epoch refers to the number of times the entire dataset is learned once, and the most efficient maximum epoch setting is required to end learning. The point at which the loss value converged to zero as much as possible was selected as the maximum epoch value. The learning rate is a constant value obtained by multiplying the error by the partial differential value with a weight, and if the initial learning rate is too large, the point where the error is minimized may not be found and diverged. The initial learning rate is set and the learning rate is lowered every number of times designated as learn rate drop period to proceed with more detailed learning. The dropout method was used to randomly ignore some of the input paths of the cell during the training of the deep-learning model. The purpose of this method is to regulate the deep-learning model to be less sensitive to the weights of specific inputs and less prone to overfit the training data. The computational cost of obtaining the loss function value for each training dataset is high. To reduce this cost, the mini-batch calculates the average loss function value by extracting data from the population based on the size of the mini-batch. The random search method has been proposed so that the LSTM network's hyper-parameters can be obtained automatically. The random search method is performed by randomly selecting arbitrary hyper-parameter values within a specific range. It had been known that the advantage of this method is reducing the number of unnecessary repetitions [34]. Based on the prediction error of the LSTM model, the model will find suitable values for the six hyper-parameters by minimizing the error value. These hyper-parameters are selected by random search method and listed in Table 5.

TABLE 5. Selected hyper-parameters for random search-based optimization for LSTM model.

Hyper-parameter	Range	Selected value
Max epochs	100-800	300
Initial learning rate	0.001-0.005	0.005
Learn rate drop period	100-300	125
Learn rate drop factor	0-1	0.2
Mini-batch size	10-200	100
Window size	10-300	120

IV. RESULTS AND DISCUSSION

A. ESTIMATION PERFORMANCE

To evaluate the basic estimation performance of the LSTM model, the simulation of the vehicle model with no noise input data was performed assuming a vehicle traveling on a C-class road at a speed of 60 km/h for 9 s (distance of 166 m). The root mean squared error (RMSE) at the kth time instant is calculated for more rigorous analysis [35], [36].

$$RMSE(k) = \sqrt{\frac{1}{k}\sum_{i=1}^{k}(p(i) - \hat{p}(i))^2} \quad (34)$$

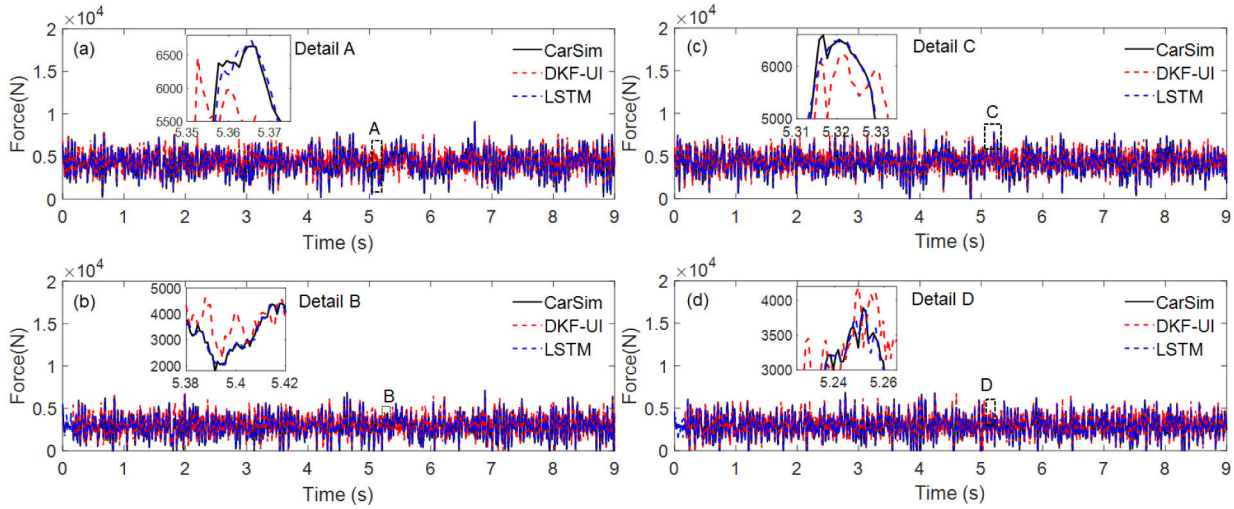

FIGURE 8. Comparison of tire normal force estimation (C-class road, 60 km/h); (a) LF, (b) LR, (c) RF, (d) RR.

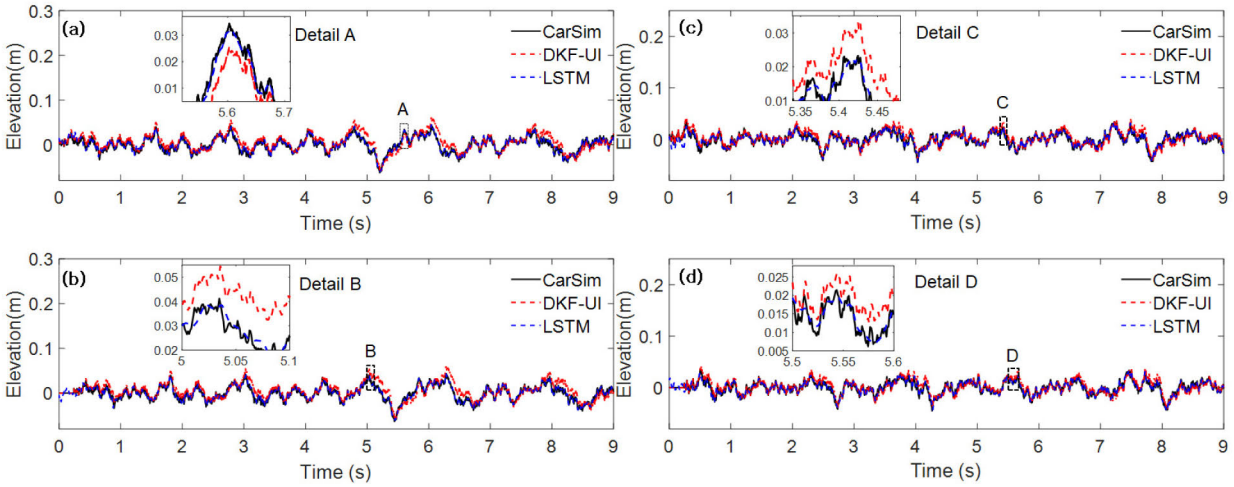

FIGURE 9. Comparison of road roughness estimation (C-class road, 60 km/h); (a) LF, (b) LR, (c) RF, (d) RR.

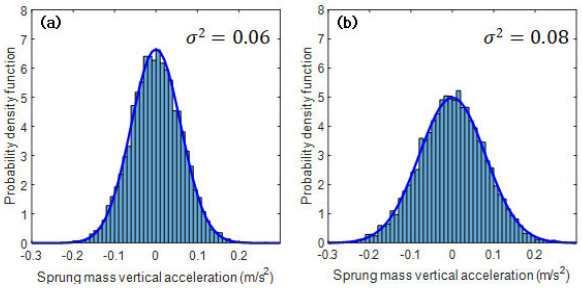

FIGURE 10. Example of Gaussian random distribution of sprung mass vertical acceleration sensor data (LSTM); (a) Case 1 (contaminated), (b) Case 2 (more contaminated).

where k is a time instant at $t = k\Delta t$, $p(i)$ and $\hat{p}(i)$ are the true (i.e., CarSim) and estimated values, respectively. The steady-state mean of RMSE (MRMSE) was then calculated to exclude the transient periods for the left front (LF) tire, right front (RF) tire, left rear (LR) tire, and right rear (RR) tire, as shown in Figure 8 and 9. The absolute MRMSE of the normal force and road roughness for the LSTM model were lower than the DKF-UI, as shown in Table 6, which implies that the LSTM model is more accurate than that of the DKF-UI model. The computation time is calculated and compared to identify the lower computational burden of the LSTM model under NVIDIA DGX STATION (Future Automotive Intelligent Electronics Core Technology Center, Republic of Korea). The computation time of the LSTM model is 0.921 s in a simulation time of 9 s, whereas the computation time of DKF-UI is 6.32 s, which indicates that the LSTM model is more lightweight and suitable for real-time control applications.

B. ROBUSTNESS ANALYSIS

The robustness of the proposed LSTM model under noise and parametric model uncertainty is analyzed by introducing the

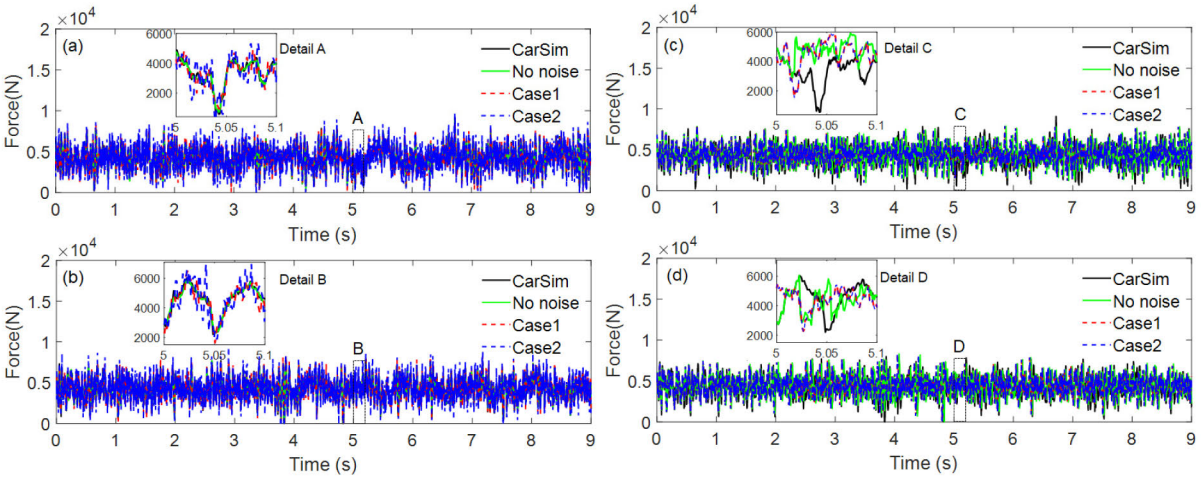

FIGURE 11. Comparison of tire normal force estimation for different sensor noise levels; (a) LF, LSTM, (b) RF, LSTM, (c) LF, DKF-UI, (d) RF, DKF-UI.

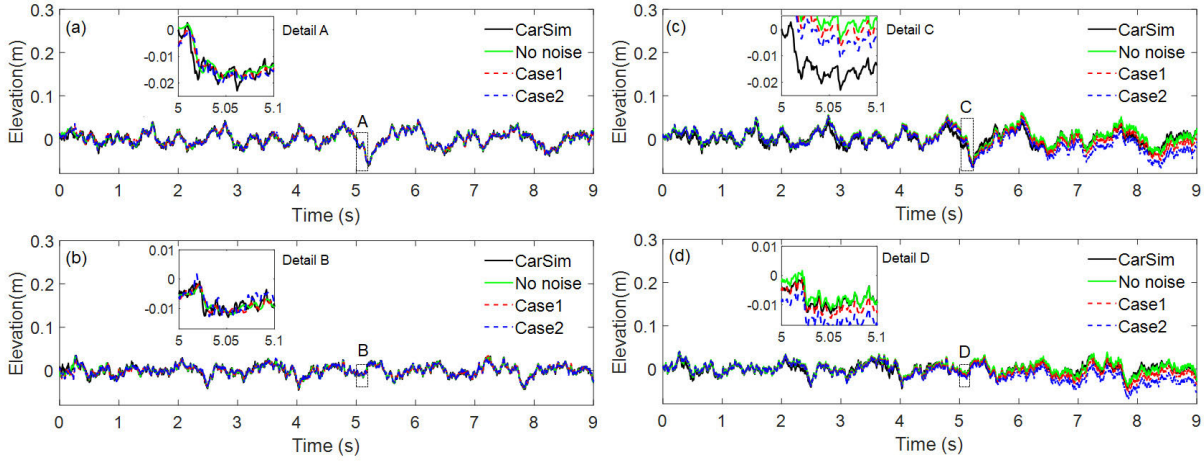

FIGURE 12. Comparison of road roughness estimation for different sensor noise levels; (a) LF, LSTM, (b) RF, LSTM, (c) LF, DKF-UI, (d) RF, DKF-UI.

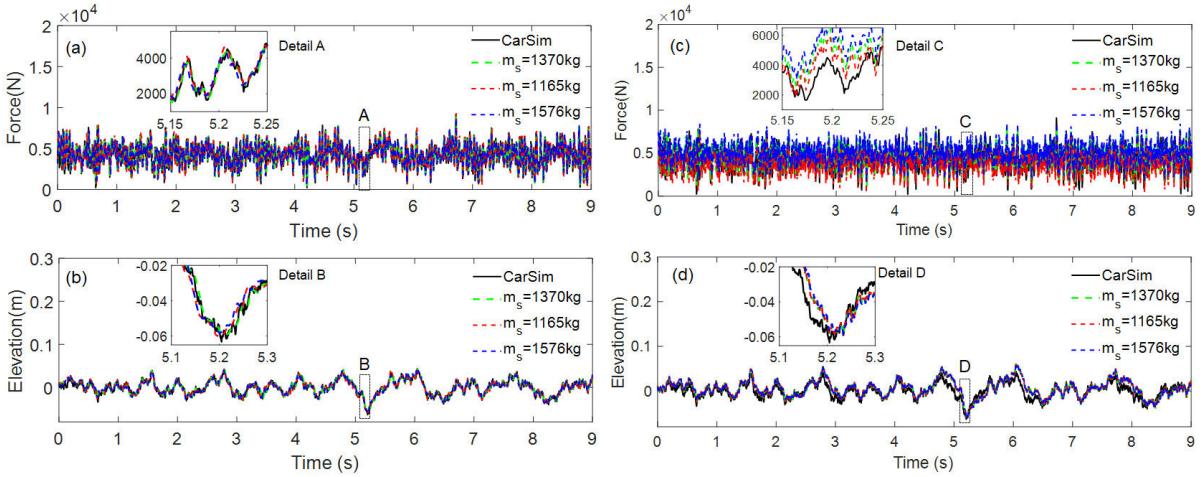

FIGURE 13. Comparison of estimation results for vehicle mass uncertainty (LF), (a) LSTM, tire normal force, (b) LSTM, road roughness, (c) DKF-UI, tire normal force, (d) DKF-UI, road roughness.

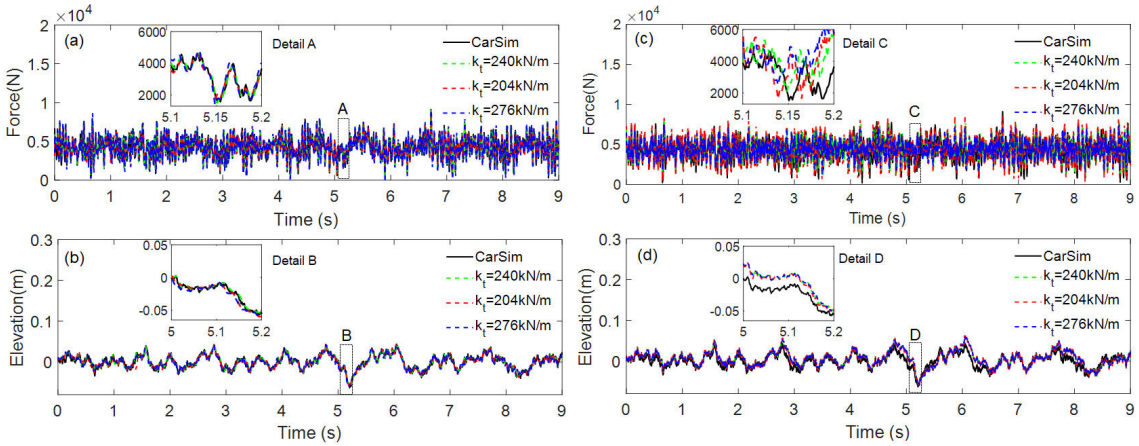

FIGURE 14. Comparison of estimation results for tire stiffness uncertainty (LF), (a) LSTM, tire normal force, (b) LSTM, road roughness, (c) DKF-UI, tire normal force, (d) DKF-UI, road roughness.

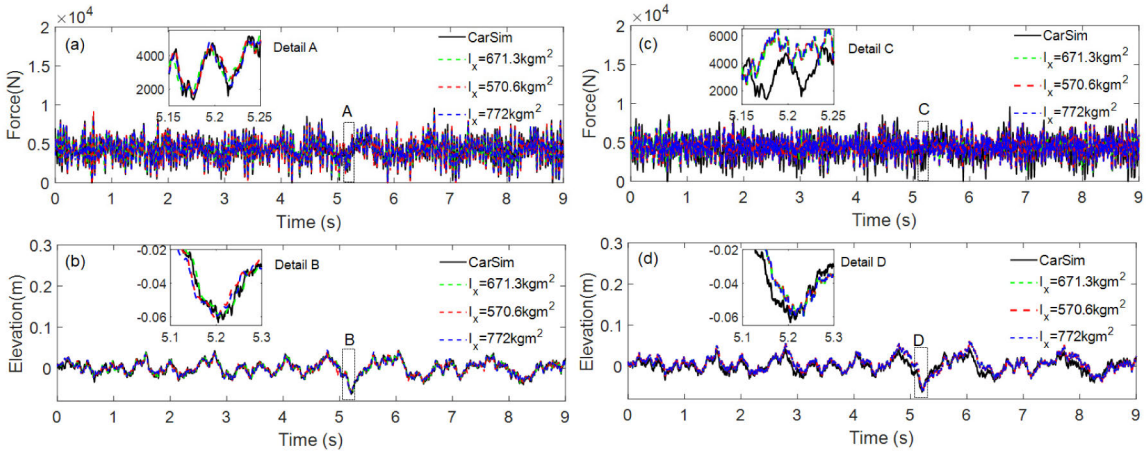

FIGURE 15. Comparison of estimation results for moment of inertia uncertainty (LF), (a) LSTM, tire normal force, (b) LSTM, road roughness, (c) DKF-UI, tire normal force, (d) DKF-UI, road roughness.

TABLE 6. Comparison of MRMSE (C-class road, 60 km/h).

	LSTM		DKF-UI	
Tire	Normal force	Road roughness	Normal force	Road roughness
LF	263.08	0.00475	913.19	0.00860
LR	239.05	0.00459	942.92	0.00863
RF	236.03	0.00491	867.86	0.00549
RR	225.46	0.00468	791.86	0.00551

perturbation of sensor noises and main parameters. Because the sensor information will be inherently contaminated by electrical noises, the effect of electrical noise on the estimation performance was examined. The white Gaussian random noise was added to all sensor data. For example, a probability density function of sprung mass vertical acceleration including white Gaussian random noise is shown in Figure 10. Because the random noise (error) distribution can be fitted to a normal Gaussian distribution with the variance ($\sigma^2 = 0.06$, Case 1), as shown in Figure 10 (a), it was confirmed by white Gaussian random noise. An original random noise has been modified to produce the more contaminated Gaussian noise ($\sigma^2 = 0.08$, Case 2), as shown in Figure 10 (b). The variance values of other input data were also added. For example, roll rate, sprung mass vertical velocity, roll rate, and pitch acceleration for Case 1 were 0.3, 0.02, 0.2, and 0.2 respectively. The proposed LSTM model seems to be robust against the Gaussian random noise extracted from all sensor data because the estimation results appeared to be similar to CarSim and DKF-UI models, as shown in Figure 11, 12. Unlike the DKF-UI model, the LSTM model learns to extract high-level features from data (i.e., cell state c_t and hidden state h_t) and convert them into the values of interest. The LSTM model is thus trained to focus on relevant information within the input time series data, resulting in filtering out unwanted noises.

The robustness of the proposed LSTM model under parametric uncertainty such as vehicle mass was examined. Because the sprung mass (i. e., vehicle mass) depends on the number of passengers, the vehicle mass is one of the significant model uncertainties. The nominal sprung mass (1370 kg) was perturbed by -15% (1165 kg) and $+15\%$ (1576 kg), respectively, as shown in Figure 13. The estimation with perturbed tire stiffness was also evaluated because the

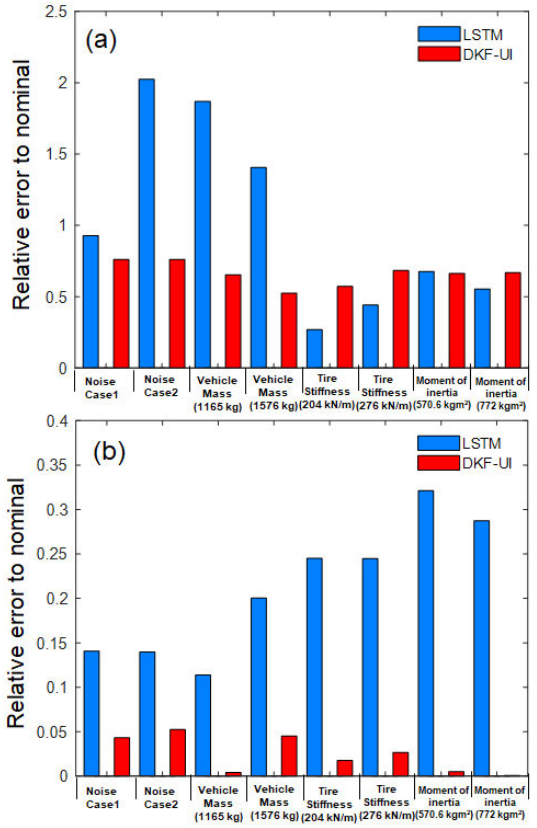

FIGURE 16. Relative errors to nominal under noise and parametric uncertainties (LF); (a) tire normal force, (b) road roughness.

relationship between the tire vertical stiffness and pressure can be assumed to be linear characteristics under the normal operation conditions (150 ∼300 *kPa*) and the tire stiffness also can be one of the significant model uncertainties when the tire inflation pressure varies [37]. The nominal tire stiffness (240 *kN/m*) was then perturbed by −15% (204 *kN/m*) and +15% (276 *kN/m*), respectively, as shown in Figure 14. The nominal moment of inertia for rolling (671.3 kgm^2) was also perturbed by −15% (570.6 kgm^2) and +15% (772 kgm^2) because it can be changed by vehicle loads and geometric variables such as roll axis, as shown in Figure 15. The same parametric uncertainties (i.e., perturbations) used for the LSTM model were also applied to the DKF-UI model. The estimation results demonstrated the advantage of proposed model-free LSTM model because the results appeared to be similar to CarSim under various parametric uncertainties to a reasonable extent.

To further investigate the robustness of the proposed LSTM model under noise and parametric uncertainties, the relative error to nominal (i. e., normalized performance measure) is quantitatively calculated and compared to the DKF-UI model.

$$\text{Relative Error} = \frac{|MRMSE_{\text{Perturbed}} - MRMSE_{\text{Nominal}}|}{MRMSE_{\text{Nominal}}} \quad (35)$$

Because similar behavior is observed in all tires, the values of the relative error to nominal for the only LF tire are illustrated in Figure 16. The estimation performance of the LSTM model for tire normal force is similar to DKF-UI except for vehicle mass uncertainty. For road roughness, the LSTM model seems to be more sensitive to noise and parametric uncertainties, compared with the DKF-UI model because road input is completely assumed as unknown input for the LSTM model whereas DKF-UI considers unknown input estimation step in Eq. (18). However, note that the performance measure is the relative error to the nominal affected by the denominator in Eq. (35) ($MRMSE_{\text{Nominal}}$, the absolute MRMSE). The LSTM model seems to be directly affected by the training data and the parameter perturbations beyond the training limit. Such limitations can be addressed by utilizing more advanced techniques such as the attention mechanism [38], [14] and physics-informed loss functions [39] that can better guide the networks to learn the vehicle dynamics from training data.

C. EXTRAPOLATION CAPABILITY

Because most deep learning models are fit to a response variable within a trained range, this may lead to degraded performance when it fits an actual response variable outside the ranges and the extrapolation capability of the proposed LSTM model should be accordingly examined. In this study, the estimation results for two non-stationary road inputs (i. e., not trained ranges; different road class and vehicle velocity) are evaluated and analyzed. The road class is initially set to be C-class and suddenly varied to D-class (i. e., not trained) for 5 s (Case 1), and quickly recovered to the original C-class road, as shown in Figure 17. Because the road roughness is typically considered as a non-stationary random variable when traveling at variable velocities, the MRMSE for different vehicle velocity scenarios was also evaluated. The vehicle velocity is initially set to be 60 km/h and suddenly accelerated to 70 km/h and remained for 5 s (i. e., not trained), and quickly recovered to 60 km/h (Case 2), as shown in Figure 18.

The robustness of the LSTM model under non-stationary road conditions seems to be qualitatively similar to Casim and DKF-UI model, which implies that the LSTM model exhibited the fundamental capability of extrapolating to out-of-distributed data. The proposed LSTM model did not overfit the training data and instead learned the vehicle dynamics directly from data, as shown in Figures 18 and 19. However, the LSTM model seems to be more sensitive to non-stationary road conditions except for Case 1 (road roughness, DFK-UI) in terms of the relative error to nominal (i. e., C-class road, 60 km/h, Table 6), as shown in Figure 19. DFK-UI appeared to be sensitive to the road roughness variation when Q and R are not optimally tuned again for D-class.

For the implementation of the LSTM model to real in-vehicle tests, the new model will be created based on the proposed LSTM model and real measured sensor data under free-ride driving conditions, including various driving speed intervals and road conditions, which is called transfer learning techniques widely used to transfer the trained knowledge to real-world. As feasibility has been proven through the simulation, we aim to utilize our pre-trained model and

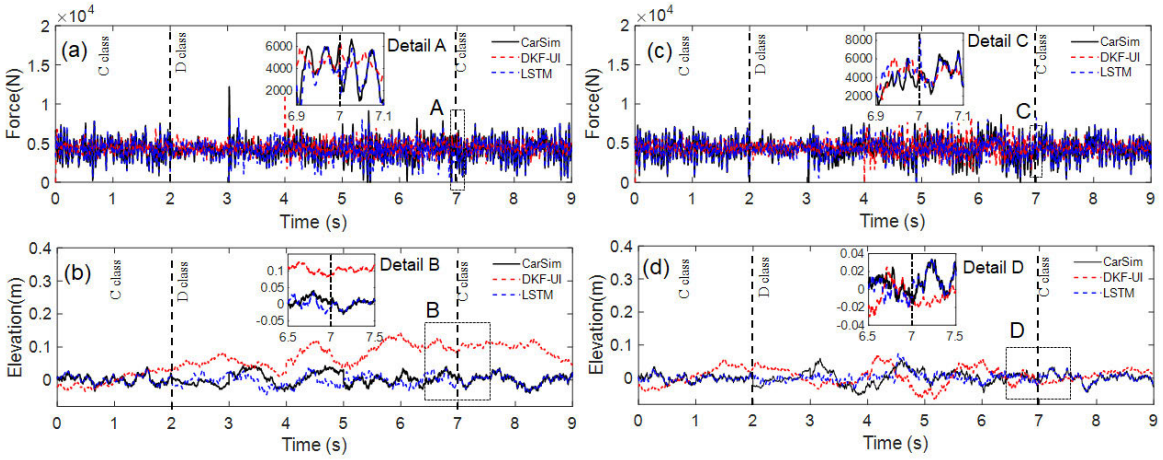

FIGURE 17. Comparison of estimation results for non-stationary road conditions (C→D→C class); (a) tire normal force of LF, (b) road roughness of LF, (c) tire normal force of RF, and (d) road roughness of RF.

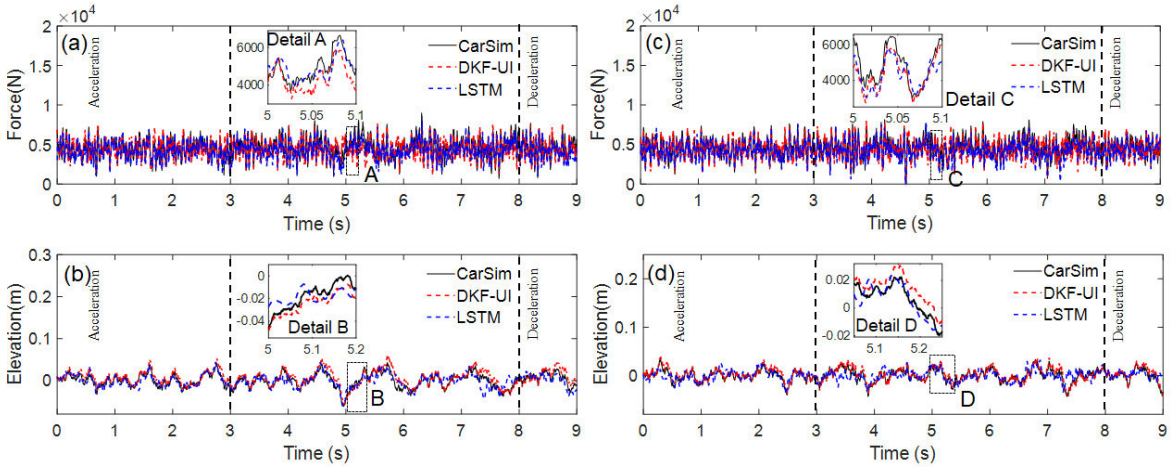

FIGURE 18. Comparison of estimation results for non-stationary road conditions (60 km/h→accelerating→70 km/h → decelerating); (a) tire normal force of LF, (b) road roughness of LF, (c) tire normal force of RF, and (d) road roughness of RF.

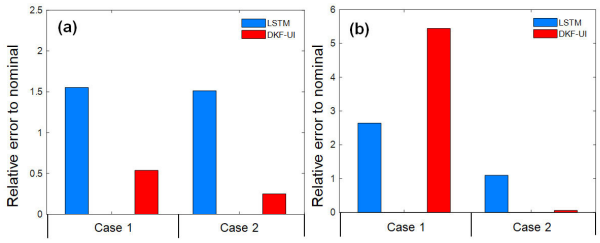

FIGURE 19. Comparison of relative errors to nominal (C-class road, 60 km/h) under non-stationary road conditions (LF); (a) tire normal force, (b) road roughness.

incorporate transfer learning strategies to circumvent the massive amount of real in-vehicle sensor data required for re-training [40].

V. CONCLUSION

In this study, the road roughness and tire normal force of the full car model (i. e, four wheels) were successfully estimated using a deep learning-based LSTM model. The main contributions of this study are summarized as follows.

- First, we conclude that the proposed model-free LSTM model is a more lightweight and efficient model to simultaneously estimate the road roughness and tire normal force by comparing the MRMSE and computation time to the DKF-UI model. Thus, the proposed model can be one of the promising alternative means to simultaneously estimate the road roughness and tire normal force when the computational cost is a significant factor.
- Secondly, although the DKF-UI algorithm had a good average performance in terms of the relative error to nominal, some limitations were observed because the nonlinear full car model used for DKF-UI is assumed by a linear model. This limitation can be addressed by using the LSTM model because neural networks can be trained by considering tire or suspension nonlinearity.
- Lastly, another advantage of using the LSTM model is that only five sensors for measured sprung mass information are used; therefore, it does not require complex physical models. With these advantages, the proposed model can be applied to an active suspension system to

create a compensation moment to prevent load transfer, increasing the stability of the vehicles.

Overall, it is necessary to improve the robustness of the LSTM model against noise and parametric uncertainties. For

$$A_c = \begin{bmatrix} A_1 & A_2 \\ A_3 & A_4 \end{bmatrix}$$

$$A_1 = \begin{bmatrix} 0 & 1 & 0 & 0 & 0 & 0 & 0 & 0 \\ \frac{-(k_{s1}+k_{tf})}{m_{u1}} & \frac{-c_{s1}}{m_{u1}} & 0 & 0 & 0 & 0 & 0 & 0 \\ 0 & 0 & 0 & 1 & 0 & 0 & 0 & 0 \\ 0 & 0 & \frac{-(k_{s2}+k_{tr})}{m_{u2}} & \frac{-c_{s2}}{m_{u2}} & 0 & 0 & 0 & 0 \\ 0 & 0 & 0 & 0 & 0 & 1 & 0 & 0 \\ 0 & 0 & 0 & 0 & \frac{-(k_{s3}+k_{tr})}{m_{u3}} & \frac{-c_{s3}}{m_{u3}} & 0 & 0 \\ 0 & 0 & 0 & 0 & 0 & 0 & 0 & 1 \\ 0 & 0 & 0 & 0 & 0 & 0 & \frac{-(k_{s4}+k_{tr})}{m_{u4}} & \frac{-c_{s4}}{m_{u4}} \end{bmatrix}$$

$$A_2 = \begin{bmatrix} 0 & 0 & 0 & 0 & 0 & 0 \\ \frac{k_{s1}b_1}{m_{u1}} & \frac{c_{s1}b_1}{m_{u1}} & \frac{-k_{s1}a_1}{m_{u1}} & \frac{-c_{s1}a_1}{m_{u1}} & \frac{k_{s1}}{m_{u1}} & \frac{c_{s1}}{m_{u1}} \\ 0 & 0 & 0 & 0 & 0 & 0 \\ \frac{k_{s2}b_1}{m_{u2}} & \frac{c_{s2}b_1}{m_{u2}} & \frac{k_{s2}a_2}{m_{u2}} & \frac{c_{s2}a_2}{m_{u2}} & \frac{k_{s2}}{m_{u2}} & \frac{c_{s2}}{m_{u2}} \\ 0 & 0 & 0 & 0 & 0 & 0 \\ \frac{-k_{s3}b_2}{m_{u3}} & \frac{-c_{s3}b_2}{m_{u3}} & \frac{k_{s3}a_2}{m_{u3}} & \frac{c_{s3}a_2}{m_{u3}} & \frac{k_{s3}}{m_{u3}} & \frac{c_{s3}}{m_{u3}} \\ 0 & 0 & 0 & 0 & 0 & 0 \\ \frac{-k_{s4}b_2}{m_{u4}} & \frac{-c_{s4}b_2}{m_{u4}} & \frac{-k_{s4}a_1}{m_{u4}} & \frac{-c_{s4}a_1}{m_{u4}} & \frac{k_{s4}}{m_{u4}} & \frac{c_{s4}}{m_{u4}} \end{bmatrix}$$

$$A_3 = \begin{bmatrix} 0 & 0 & 0 & 0 & 0 & 0 & 0 & 0 \\ \frac{k_{s1}b_1}{I_x} & \frac{c_{s1}b_1}{I_x} & \frac{k_{s2}b_1}{I_x} & \frac{c_{s2}b_1}{I_x} & -\frac{k_{s3}b_2}{I_x} & -\frac{c_{s3}b_2}{I_x} & -\frac{k_{s4}b_2}{I_x} & -\frac{c_{s4}b_2}{I_x} \\ 0 & 0 & 0 & 0 & 0 & 0 & 0 & 0 \\ -\frac{k_{s1}a_1}{I_y} & -\frac{c_{s1}a_1}{I_y} & \frac{k_{s2}a_2}{I_y} & \frac{c_{s2}a_2}{I_y} & \frac{k_{s3}a_2}{I_y} & \frac{c_{s3}a_2}{I_y} & -\frac{k_{s4}a_1}{I_y} & -\frac{c_{s4}a_1}{I_y} \\ 0 & 0 & 0 & 0 & 0 & 0 & 0 & 0 \\ \frac{k_{s1}}{m_s} & \frac{c_{s1}}{m_s} & \frac{k_{s2}}{m_s} & \frac{c_{s2}}{m_s} & \frac{k_{s3}}{m_s} & \frac{c_{s3}}{m_s} & \frac{k_{s4}}{m_s} & \frac{c_{s4}}{m_s} \end{bmatrix}$$

$$A_4 = \begin{bmatrix} 0 & 1 & 0 & 0 & 0 & 0 \\ \frac{-b_1^2K_1-b_2^2K_2}{I_x} & \frac{-b_1^2C_1-b_2^2C_2}{I_x} & \frac{vk_1-vk_2+vk_3-vk_4}{I_x} & \frac{vc_1-vc_2+vc_3-vc_4}{I_x} & \frac{-b_1K_1+b_2K_2}{I_x} & \frac{-b_1C_1+b_2C_2}{I_x} \\ 0 & 0 & 0 & 1 & 0 & 0 \\ \frac{vk_1-vk_4-vk_2+vk_3}{I_y} & \frac{vc_1-vc_4-vc_2+vc_3}{I_y} & \frac{-a_1^2K_3-a_2^2K_4}{I_y} & \frac{-a_1^2C_3-a_2^2C_4}{I_y} & \frac{a_1K_3-a_2K_4}{I_y} & \frac{a_1C_3-a_2C_4}{I_y} \\ 0 & 0 & 0 & 0 & 0 & 1 \\ \frac{-b_1K_1+b_2K_2}{m_s} & \frac{-b_1C_1+b_2C_2}{m_s} & \frac{a_1K_3-a_2K_4}{m_s} & \frac{a_1C_3-a_2C_4}{m_s} & \frac{-(K1+K2)}{m_s} & \frac{-(C1+C2)}{m_s} \end{bmatrix}$$

$$B_c = \begin{bmatrix} 0 & 0 & 0 & 0 \\ \frac{k_{tf}}{m_{u1}} & 0 & 0 & 0 \\ 0 & 0 & 0 & 0 \\ 0 & \frac{k_{tf}}{m_{u2}} & 0 & 0 \\ 0 & 0 & 0 & 0 \\ 0 & 0 & \frac{k_{tf}}{m_{u3}} & 0 \\ 0 & 0 & 0 & 0 \\ 0 & 0 & 0 & \frac{k_{tf}}{m_{u4}} \\ 0 & 0 & 0 & 0 \\ 0 & 0 & 0 & 0 \\ 0 & 0 & 0 & 0 \\ 0 & 0 & 0 & 0 \\ 0 & 0 & 0 & 0 \\ 0 & 0 & 0 & 0 \end{bmatrix}$$

$$C = \begin{bmatrix} C_1 & C_2 \end{bmatrix}$$

$$C_1 = \begin{bmatrix} \frac{-(k_{s1}+k_{tf})}{m_{u1}} & \frac{-c_{s1}}{m_{u1}} & 0 & 0 & 0 & 0 & 0 & 0 \\ 0 & 0 & \frac{-(k_{s2}+k_{tr})}{m_{u2}} & \frac{-c_{s2}}{m_{u2}} & 0 & 0 & 0 & 0 \\ 0 & 0 & 0 & 0 & \frac{-(k_{s3}+k_{tr})}{m_{u3}} & \frac{-c_{s3}}{m_{u3}} & 0 & 0 \\ 0 & 0 & 0 & 0 & 0 & 0 & \frac{-(k_{s4}+k_{tr})}{m_{u4}} & \frac{-c_{s4}}{m_{u4}} \\ 0 & 0 & 0 & 0 & 0 & 0 & 0 & 0 \\ \frac{k_{s1}}{m_s} & \frac{c_{s1}}{m_s} & \frac{k_{s2}}{m_s} & \frac{c_{s2}}{m_s} & \frac{k_{s3}}{m_s} & \frac{c_{s3}}{m_s} & \frac{k_{s4}}{m_s} & \frac{c_{s4}}{m_s} \\ \frac{k_{s1}b_1}{I_x} & \frac{c_{s1}b_1}{I_x} & \frac{k_{s2}b_1}{I_x} & \frac{c_{s2}b_1}{I_x} & \frac{-k_{s3}b_2}{I_x} & \frac{-c_{s3}b_2}{I_x} & \frac{-k_{s4}b_2}{I_x} & \frac{-c_{s4}b_2}{I_x} \\ \frac{-k_{s1}a_1}{I_y} & \frac{-c_{s1}a_1}{I_y} & \frac{k_{s2}a_2}{I_y} & \frac{c_{s2}a_2}{I_y} & \frac{k_{s3}a_2}{I_y} & \frac{c_{s3}a_2}{I_y} & \frac{-k_{s4}a_1}{I_y} & \frac{-c_{s4}a_1}{I_y} \end{bmatrix}$$

$$C_2 = \begin{bmatrix} \frac{k_{s1}b_1}{m_{u1}} & \frac{c_{s1}b_1}{m_{u1}} & \frac{-k_{s1}a_1}{m_{u1}} & \frac{-c_{s1}a_1}{m_{u1}} & \frac{k_{s1}}{m_{u1}} & \frac{c_{s1}}{m_{u1}} \\ \frac{k_{s2}b_1}{m_{u2}} & \frac{c_{s2}b_1}{m_{u2}} & \frac{k_{s2}a_2}{m_{u2}} & \frac{c_{s2}a_2}{m_{u2}} & \frac{k_{s2}}{m_{u2}} & \frac{c_{s2}}{m_{u2}} \\ \frac{-k_{s3}b_2}{m_{u3}} & \frac{-c_{s3}b_2}{m_{u3}} & \frac{k_{s3}a_2}{m_{u3}} & \frac{c_{s3}a_2}{m_{u3}} & \frac{k_{s3}}{m_{u3}} & \frac{c_{s3}}{m_{u3}} \\ \frac{-k_{s4}b_2}{m_{u4}} & \frac{-c_{s4}b_2}{m_{u4}} & \frac{k_{s4}a_1}{m_{u4}} & \frac{-c_{s4}a_1}{m_{u4}} & \frac{k_{s4}}{m_{u4}} & \frac{c_{s4}}{m_{u4}} \\ 0 & 0 & 0 & 0 & 1 & 0 \\ \frac{-b_1K_1+b_2K_2}{m_s} & \frac{-b_1C_1+b_2C_2}{m_s} & \frac{a_1K_3-a_2K_4}{m_s} & \frac{a_1C_3-a_2C_4}{m_s} & \frac{-(K1+K2)}{m_s} & \frac{-(C1+C2)}{m_s} \\ \frac{-b_1^2K_1-b_2^2K_2}{I_x} & \frac{-b_1^2C_1-b_2^2C_2}{I_x} & \frac{vk_1-vk_2+vk_3-vk_4}{I_x} & \frac{vc_1-vc_2+vc_3-vc_4}{I_x} & \frac{-b_1K_1+b_2K_2}{I_x} & \frac{-b_1C_1+b_2C_2}{I_x} \\ \frac{vk_1-vk_4-vk_2+vk_3}{I_y} & \frac{vc_1-vc_4-vc_2+vc_3}{I_y} & \frac{-a_1^2K_3-a_2^2K_4}{I_y} & \frac{-a_1^2C_3-a_1^2C_4}{I_y} & \frac{a_1K_3-a_2K_4}{I_y} & \frac{a_1C_3-a_2C_4}{I_y} \end{bmatrix}$$

$$D = \begin{bmatrix} \frac{k_{tf}}{m_{u1}} & 0 & 0 & 0 \\ 0 & \frac{k_{tf}}{m_{u2}} & 0 & 0 \\ 0 & 0 & \frac{k_{tf}}{m_{u3}} & 0 \\ 0 & 0 & 0 & \frac{k_{tf}}{m_{u4}} \\ 0 & 0 & 0 & 0 \\ 0 & 0 & 0 & 0 \\ 0 & 0 & 0 & 0 \\ 0 & 0 & 0 & 0 \end{bmatrix}$$

$$K_1 = k_{s1} + k_{s2} \quad K_2 = k_{s3} + k_{s4}\ K_3 = k_{s1} + k_{s4}\ K_4 = k_{s2} + k_{s3}$$
$$C_1 = c_{s1} + c_{s2} \quad C_2 = c_{s3} + c_{s4}\ C_3 = c_{s1} + c_{s4}\ C_4 = c_{s2} + c_{s3}$$
$$vk_1 = a_1b_1k_{s1} \quad vk_2 = a_2b_1k_{s2}\ vk_3 = a_2b_2k_{s3}\ vk_4 = a_1b_2k_{s4}$$
$$vc_1 = a_1b_1c_{s1} \quad vc_2 = a_2b_1c_{s2}\ vc_3 = a_2b_2c_{s3}\ vc_4 = a_1b_2c_{s4}$$

the future research direction, we will continue to address some ongoing issues. In particular, the LSTM model will be implemented in real vehicles, and its estimation performance is compared with the simulation results because the CarSim model does not consider the sensor mounting inaccuracy, abnormal wear, unexpected payload, passenger's driving habits, etc. Another scope of future work includes a better understanding of the black box-based LSTM model's mechanisms, thus improving the reliability and robustness of the proposed model. Although our results indicate that the LSTM model is particularly sensitive to parametric perturbations, possible reasons remain to be discovered and could be addressed by using interpretation algorithms.

APPENDIX

Detailed expressions of the system matrix (A_c), input matrix (B_c), output matrix (C), and feedforward matrix (D) introduced in Section III-B are given as shown at the bottom of the previous page and the page.

REFERENCES

[1] T. Merker, G. Girres, and O. Thriemer, "Active body control (ABC) the daimlerchrysler active suspension and damping system," SAE, Warrendale, PA, USA, Tech. Paper 2002-21-0054, 2002.

[2] Y. Lian, Y. Zhao, L. Hu, and Y. Tian, "Cornering stiffness and sideslip angle estimation based on simplified lateral dynamic models for four-in-wheel-motor-driven electric vehicles with lateral tire force information," *Int. J. Autom. Technol.*, vol. 16, no. 4, pp. 669–683, 2015.

[3] H. Hamann, J. K. Hedrick, S. Rhode, and F. Gauterin, "Tire force estimation for a passenger vehicle with the unscented Kalman filter," in *Proc. IEEE Intell. Veh. Symp. Conf.*, Dearborn, MI, USA, Oct. 2014, pp. 814–819.

[4] J.-S. Oh and S.-B. Choi, "Ride quality control of a full vehicle suspension system featuring magnetorheological dampers with multiple orifice holes," *Frontiers Mater.*, vol. 6, p. 8, Feb. 2019.

[5] J. Jiang, M. Seaid, M. S. Mohamed, and H. Li, "Inverse algorithm for real-time road roughness estimation for autonomous vehicles," *Arch. Appl. Mech.*, vol. 90, no. 6, pp. 1333–1348, 2020.

[6] J.-Y. Han, A. Chen, and Y.-T. Lin, "Image-based approach for road profile analyses," *J. Surveying Eng.*, vol. 142, no. 1, Feb. 2016, Art. no. 06015003.

[7] J.-H. Lee, S.-H. Lee, D.-K. Kang, S.-D. Na, and W.-S. Yoo, "Development of a 3D road profile measuring system for unpaved road severity analysis," *Int. J. Precis. Eng.*, vol. 18, no. 2, p. 155 162, 2017.

[8] S.-W. Kang, J.-S. Kim, and G.-W. Kim, "Road roughness estimation based on discrete Kalman filter with unknown input," *Veh. Syst. Dyn.*, vol. 57, no. 10, pp. 1530–1544, 2019.
[9] G.-W. Kim, S.-W. Kang, J.-S. Kim, and J.-S. Oh, "Simultaneous estimation of state and unknown road roughness input for vehicle suspension control system based on discrete Kalman filter," *Proc. Inst. Mech. Eng. D, J. Automob. Eng.*, vol. 234, no. 6, pp. 1610–1622, 2020.
[10] Y. Qin, C. Wei, X. Tang, N. Zhang, M. Dong, and C. Hu, "A novel nonlinear road profile classification approach for controllable suspension system: Simulation and experimental validation," *Mech. Syst. Signal Process.*, vol. 125, p. 79 98, 2019.
[11] Basavaraju, J. Du, F. Zhou, and J. Ji, "A machine learning approach to road surface anomaly assessment using smartphone sensors," *IEEE Sensors J.*, vol. 20, no. 5, p. 2635 2647, 2019.
[12] Y. Qin, R. Langari, and L. Gu, "The use of vehicle dynamic response to estimate road profile input in time domain," in *Proc. Dyn. Modeling Diag. Biomed. Syst., Dyn. Control Wind Energy Syst.*, Oct. 2014, pp. 1–5.
[13] H. M. Ngwangwa, P. S. Heyns, H. G. A. Breytenbach, and P. S. Els, "Reconstruction of road defects and road roughness classification using artificial neural networks simulation and vehicle dynamic responses: Application to experimental data," *J. Terramechanics*, vol. 53, pp. 1–18, Jun. 2014.
[14] G. Kim, S. Y. Lee, J.-S. Oh, and S. Lee, "Deep learning-based estimation of the unknown road profile and state variables for the vehicle suspension system," *IEEE Access*, vol. 9, pp. 13878–13890, 2021.
[15] Y. Zhang and J. Yi, "Static tire/road stick-slip interactions: Analysis and experiments," *IEEE ASME Trans. Mechatron.*, vol. 19, no. 6, pp. 1940–1950, 2013.
[16] L. R. Ray, "Nonlinear state and tire force estimation for advanced vehicle control," *IEEE Trans. Control Syst. Technol.*, vol. 3, no. 1, pp. 117–124, 1995.
[17] B. Samadi, R. Kazemi, K. Y. Nikravesh, and M. Kabganian, "Real-time estimation of vehicle state and tire-road friction forces," in *Proc. Amer. Control Conf.*, Arlington VA, USA, 2001, p. 3318.
[18] M. Doumiati, A. Victorino, A. Charara, G. Baffet, and D. Lechner, "An estimation process for vehicle wheel-ground contact normal forces," in *Proc. 17th Int. IFAC Conf.*, 2008, pp. 7110–7115.
[19] K. Jiang, A. Pavelescu, A. Victorino, and A. Charara, "Estimation of vehicle's vertical and lateral tire forces considering road angle and road irregularity," in *Proc. 17th Int. IEEE Conf. Intell. Transp. Syst. (ITSC)*, Qingdao China, Oct. 2014, p. 342.
[20] J. J. Castillo, J. A. Cabrera, A. J. Guerra, and A. Simon, "A novel electrohydraulic brake system with tire-road friction estimation and continuous brake pressure control," *IEEE Trans. Ind. Electron.*, vol. 63, no. 3, pp. 1863–1875, Oct. 2015.
[21] H. Tsunashima, M. Murakami, and J. Miyataa, "Vehicle and road state estimation using interacting multiple model approach," *Veh. Syst. Dyn.*, vol. 44, no. 1, pp. 750–758, 2006.
[22] J. Rath, K. C. Veluvolu, and M. Defoort, "Simultaneous estimation of road profile and tire road friction for automotive vehicle," *IEEE Trans. Veh. Technol.*, vol. 64, no. 10, pp. 4461–4471, Nov. 2014.
[23] Z. Wang, Y. Qin, L. Gu, and M. Dong, "Vehicle system state estimation based on adaptive unscented Kalman filtering combing with road classification," *IEEE Access*, vol. 5, p. 27786 27799, 2017.
[24] C*arSim (V 9.0) Reference Manual*, Mech. Simul. Corp., Ann Arbor, MI, USA, 2006.
[25] S. Hochreiter and J. Urgen Schmidhuber, "Long short-term memory," *Neural Comput.*, vol. 9, no. 8, pp. 1735–1780, 1997.
[26] J. Van Ginkel, "Estimating the tire-road friction coefficient based on tire force measurements," M.S. thesis, Dept. Biomed. Eng., Delft Univ., Delft, The Netherlands, 2014.
[27] K. R. Khanse, Y. Siramdasu, and S. Taheri, "Development of a Simulink-CarSim interaction package for ABS simulation of discrete tire models," *Tire Sci. Technol.*, vol. 44, no. 1, pp. 2–21, Jan. 2016.
[28] D. Hrovat, "Survey of advanced suspension developments and related optimal control applications," *Automatica*, vol. 33, no. 10, pp. 1781–1817, 1997.
[29] S. Ruan, C. Tang, X. Zhou, Z. Jin, S. Chen, H. Wen, H. Liu, and D. Tang, "Multi-pose face recognition based on deep learning in unconstrained scene," *Appl. Sci.*, vol. 10, no. 13, p. 4669, Jul. 2020.
[30] J. Ba and D. Kingma, "Adam: A method for stochastic optimization," in *Proc. 3rd Int. Conf. Learn. Represent.*, vol. 2015, pp. 127–142.
[31] D. S. Yoon, G. W. Kim, and S. B. Choi, "Response time of magnetorheological dampers to current inputs in a semi-active suspension system: Modeling, control and sensitivity analysis," *Mech. Syst. Signal Process.*, vol. 146, Oct. 2021, Art. no. 106999.
[32] R. Rajamani, *Vehicle Dynamics and Control*. Boston, MA, USA: Springer, 2011.
[33] G. Rill, *Road Vehicle Dynamics: Fundamentals and Modeling*. Boca Raton, FL, USA: CRC Press, 2011.
[34] J. Bergstra and Y. Bengio, "Random search for hyper-parameter optimization," *J. Mach. Learn. Res.*, vol. 13, no. 2, pp. 281–305, 2012.
[35] M. Khan, N. Salman, A. Ali, A. Khan, and A. Kemp, "A comparative study of target tracking with Kalman filter, extended Kalman filter and particle filter using received signal strength measurements," in *Proc. Int. ICET Conf.*, vol. 2015, pp. 1–6.
[36] W. S. Rosenthal, A. M. Tartakovsky, and Z. Huang, "Ensemble Kalman filter for dynamic state estimation of power grids stochastically driven by time-correlated mechanical input power," *IEEE Trans. Power Syst.*, vol. 33, no. 4, pp. 3701–3710, 2017.
[37] D.-H. Lee, D.-S. Yoon, and G.-W. Kim, "New indirect tire pressure monitoring system enabled by adaptive extended Kalman filtering of vehicle suspension systems," *Electronics*, vol. 10, no. 11, p. 1359, Jun. 2021.
[38] A. Vaswani, N. Shazeer, and N. Parmar, "Attention is all you need," in *Proc. Adv. Neural Inf. Process. Syst.*, vol. 30, 2017, pp. 1–11.
[39] G. Karniadakis, I. Kevrekidis, and L. Lu, "Physics-informed machine learning," *Nat. Rev. Phys.*, vol. 3, no. 6, pp. 422–440, 2021.
[40] L. Torrey and J. Shavlik, "Transfer learning," *Handbook of Research on Machine Learning Applications and Trends: Algorithms, Methods, and Techniques*. Hershey, PA, USA: IGI Global, 2010, pp. 242–264.

SUNG JIN IM received the B.S. degree in mechanical engineering from Kongju National University, Cheonan, South Korea, in 2020. He is currently pursuing the M.S. degree with the Control Systems and Mechatronics Laboratory, Inha University, South Korea. His research interests include Kalman filters, parameter estimation, vehicle control, and their industrial applications.

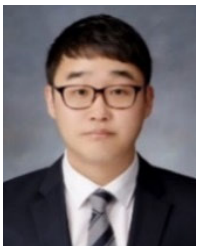

JONG SEOK OH received the B.S., M.S., and Ph.D. degrees in mechanical engineering from Inha University, Incheon, South Korea, in 2009, 2011, and 2015, respectively. He is currently an Assistant Professor with Kongju National University. His research interests include robust controller design and control of various systems using smart actuators, such as magnetorheological and electrorheological fluids, and piezo actuators.

GI-WOO KIM received the Ph.D. degree from the Mechanical Engineering Department, Pennsylvania State University, USA, in 2009. He worked with the Hyundai Motor Company Powertrain Research and Development Center, from 1996 to 2004, and at the Mechanical Engineering Department, University of Michigan, from 2009 to 2011. He worked as an Assistant Professor at Kyungpook National University, from 2011 to 2015. He has been working as a Professor with Inha University, since 2015. His research interests include data-driven mechanical engineering: machine learning, measurement and control, vehicular electronics, and sensor fusion for future mobility.